Materials Transactions, Vol. 54, No. 4 (2013) pp. 456 to 465
Special Issue on Materials-System Integration for Fusion DEMO Blanket

OVERVIEW

Development of Nanostructured Tungsten Based Materials Resistant to Recrystallization and/or Radiation Induced Embrittlement

H. Kurishita[1,*], H. Arakawa[1], S. Matsuo[1], T. Sakamoto[2], S. Kobayashi[2], K. Nakai[2], G. Pintsuk[3], J. Linke[3], S. Tsurekawa[4], V. Yardley[4], K. Tokunaga[5], T. Takida[6], M. Katoh[6], A. Ikegaya[6], Y. Ueda[7], M. Kawai[8] and N. Yoshida[5]

[1]*International Research Center for Nuclear Materials Science, IMR, Tohoku University, Oarai, Ibaraki 311-1313, Japan*
[2]*Department of Materials Science and Biotechnology, Ehime University, Matsuyama 790-8577, Japan*
[3]*Forschungszentrum Jülich, EURATOM Association, 52425 Jülich, Germany*
[4]*Department of Materials Science and Engineering, Graduate School of Science and Technology, Kumamoto University, Kumamoto 860-8555, Japan*
[5]*Institute for Applied Mechanics, Kyushu University, Kasuga, Fukuoka 816-8580, Japan*
[6]*A. L. M. T. Corp., Toyama 931-8543, Japan*
[7]*Graduate School of Engineering, Osaka University, Osaka 565-0871, Japan*
[8]*Institute of Material Structure Science, High Energy Accelerator Research Organization (KEK), Tsukuba 305-0801, Japan*

Mitigation of embrittlement caused by recrystallization and radiation is the key issue of tungsten (W) based materials for use in the advanced nuclear system such as fusion reactor applications. In this paper, our nanostructured W materials development performed so far to solve the key issue is reviewed, including new original data. Firstly, the basic concept of mitigation of the embrittlement is shown. The approach to the concept has yielded ultra-fine grained, recrystallized (UFGR) W–(0.25–1.5) mass%TiC compacts containing fine TiC dispersoids (precipitates). The UFGR W–(0.25–1.5)%TiC exhibits favorable as well as unfavorable features from the viewpoints of microstructures and various thermo-mechanical properties including the response to neutron and ion irradiations. Most of the unfavorable features stem from insufficient strengthening of weak random grain boundaries (GBs) in the recrystallized state. The focal point on this study is, therefore, to develop a new microstructural modification method to significantly strengthen the random GBs. The method is designated as GSMM (GB Sliding-based Microstructural Modification) and has lead to the birth of toughened, fine-grained W–1.1%TiC in the recrystallized state (TFGR W–1.1TiC). The TFGR W–1.1TiC exhibits much improved thermo-mechanical properties. The applicability of TFGR W–1.1TiC to the divertor in ITER is discussed. [doi:10.2320/matertrans.MG201209]

(Received October 17, 2012; Accepted January 29, 2013; Published March 15, 2013)

Keywords: *tungsten, transition metal carbide, embrittlement, recrystallization, radiation, high heat loading, grain boundary, international thermonuclear experimental reactor*

1. Introduction

Tungsten (W) is currently attracting the greatest attention among materials for use as functional and structural materials in the advanced nuclear system:[1–6] W is planned to be employed as the key material in the divertor (full divertor) in ITER (International Thermonuclear Experimental Reactor) that possesses a function of extracting ashes arising from fusion reaction in the plasma. W in the divertor will be exposed to heavy thermal loads in the steady state or transient mode combined with irradiation with high energy neutron, low energy ion that will cause serious material degradation. W is also the leading candidate material of a rotating solid target receiving MW-class protons to produce intense long-pulsed neutrons for the second target of the SNS (Spallation Neutron Source) project in US and the CSNS (Chinese Spallation Neutron Source) target. The target will be irradiated with high energy protons and neutrons.

The recent recurrence of attention to W is due to its many superior properties that are never available in the other metals: Among metals, W exhibits the highest melting point (3683 K), lowest coefficient of thermal expansion, lowest anisotropy of elastic constant, lowest solubility of hydrogen isotopes, lowest sputtering yields, highest compatibility with liquid metals, much better thermal conductivity (174 W/(m·K) than that of Fe (73 W/(m·K)), high neutron yield (i.e., large mass number, high density (19.3 g/cm^3)), reduced decay heat by transmutation products, etc.

However, the utilization of W based materials is still limited to filaments, electrodes and heaters where W is used in a form of wire or sheet because fracture resistant W products are available mainly in these geometries with the optimally deformed structures achievable via heavy plastic working processes. W based bulk (thick) materials have not successfully been applied to functional and structural materials, especially in high temperature and radiation environments. This is because W exhibits intergranular embrittlement by recrystallization and/or radiation. Recrystallization in W occurs at temperatures much lower than the melting point and upon recrystallization it becomes very susceptible to cracking along grain boundaries. Radiation with high energy neutron and protons induces lattice defects in materials, thereby in most cases causing hardening and embrittlement of materials (radiation embrittlement).[7,8] Therefore, in order to take advantage of the many superior properties of W, it is necessary to significantly mitigate embrittlement by recrystallization and radiation.

The authors have recently developed a new microstructural modification method that may enable mitigation of both embrittlement by recrystallization and radiation in W and fabricated TFGR (Toughened, Fine Grained, Recrystallized)

*Corresponding author, E-mail: kurishi@imr.tohoku.ac.jp

W–1.1%TiC compacts. This paper highlights the progress in the development of TFGR W–1.1%TiC.

2. Basic Approach to Mitigation of Embrittlement by Recrystallization and Radiation

Recrystallization in W materials leads to the formation of new grain boundaries of random orientations (random grain boundaries) that are very high energy and very susceptible to cracking and these boundaries are prone to fracture as referred to as recrystallization embrittlement. The formation of random grain boundaries is attributed to strong covalence of atomic bonding in W and segregation and precipitation of gaseous interstitial elements of oxygen and nitrogen which are insoluble in the W matrix. In order to mitigate recrystallization embrittlement, it is necessary to replace the weak cohesion at random grain boundaries with a strong interatomic bond and reduce the contents of harmful impurities of oxygen and nitrogen to a negligibly small level.

Radiation embrittlement is caused mainly by increase in yield strength due to accumulation of radiation induced defects (radiation hardening). Accumulation of radiation induced defects can be suppressed by introducing a high density of sinks, such as grain boundaries and dispersoids, for the defects. Our preceding study on nanostructured Mo showed an encouraging result:[9,10] Structural changes occurring under un-equilibrium states of radiation environments lead to significant increase in ductility compared with that in the unirradiated states. This phenomenon is opposite to radiation embrittlement and regarded as radiation induced ductilization (RIDU).[11,12] RIDU can occur providing that beneficial effects of strengthening of the random grain boundaries due to radiation-enhanced and/or -induced segregation and precipitation of the constituent elements exceed the detrimental effects of radiation hardening. RIDU has so far been observed for nanostructured Mo–(0.2–1.0)%TiC with controlled temperature-cycle neutron irradiations between the lower temperature such as 473 and 573 K and higher temperature such as 673 and 773 K for several cycles.[9–12]

Given the above results and motivated with an expectation of a synonymous effect on W, we select TiC, one of the transition metal carbides (TMCs), as a dispersoid phase, and use TiC powder as the starting material. As described in chapter 3, our powder metallurgical processing method at first permits added TiC powder to decompose into Ti and C, producing the powder of a solid solution of W–Ti–C. Then, the Ti and C solutes in the W matrix react to form fine TiC precipitates. TiC exhibits a high melting point (~3520 K) and a self-adjustment capability of the lattice constant by forming a solid solution with W and leaving a non-stoichiometry of TiCx and offers strengthening effects of random grain boundaries due to precipitation of TiCx and its segregation at the grain boundaries: The occurrence of grain boundary precipitation always follows segregation of the constituents of TiC precipitate at grain boundaries. The strengthening effect by TiC addition was already reported in Mo bicrystals[13] and nanostructured Mo[14–16] and confirmed in nanostructured W[17] with small amounts of TiC additions. Therefore, it is believed that the most preferable microstructure for mitigating embrittlement by recrystallization and radiation in W is composed of a high density of both TMC dispersoids and grain boundaries that are significantly strengthened by enrichment of the TMC components with negligibly small amounts of oxygen and nitrogen impurities.

3. Ultra-Fine Grained W–(0.25–1.5)%TiC in the Recrystallized State

Ultra-fine grained compacts of W–(0.25–1.5) mass%TiC in the rcrystrallized state (hereafter designated as UFGR W–TiC) are produced by powder metallurgical methods utilizing mechanical alloying (MA)[18] and HIP (hot isostatic pressing) from the starting powders of W and TiC.[10,17] Of importance is the use of high purity powders and thorough prevention of contamination with the interstitial elements of oxygen and nitrogen contained in the atmospheres through the whole fabrication process. For this, powder treatments are always made in a well degassed glove box filled with a purified Ar or H_2 gas. The MA process facilitates the decomposition of TiC into Ti and C and produces a solid solution of W–Ti–C along with ultra-fine grains of 20–30 nm in diameter. The ultra-fine grains were, however, difficult to be maintained in the fully densified compacts after sintering because full densification requires high temperature sintering where significant grain growth would occur: When the MA treated W–0.5%TiC powder was HIPed at 1620 K, the as-HIPed compacts contained porosity of as much as 6% although it still exhibited ultra-fine grains of 50 nm in diameter.[17] Fully densified, UFGR W–TiC compacts were successfully fabricated in 2004:[19] HIPing at 1623–1673 K, approximately 2/5 of the melting point, resulted in precipitation of nano-sized dispersoids and essentially full densification without significantly increasing the grain size of the MA treated powder.

The UFGR W–TiC compacts have attracted great attention because such a nanostructure was the first to fabricate in W-based materials. Domestic and international research collaborations have revealed that the UFGR W–TiC exhibits the following features of the microstructures, mechanical and thermal properties, responses to neutron and ion irradiation, plasma exposure and high heat loading.[20–32] Since the features of UFGR W–TiC are considerably affected by the atmosphere in MA (Ar or H_2), we designate the compacts as W–TiC/Ar or W–TiC/H, which denotes the sealed gas in the MA process, Ar or H_2, respectively.

Although the detailed description concerning W–TiC/Ar and W–TiC/H is provided in the followings, it is important to at first answer the question "Which is useful, W–TiC/Ar or W–TiC/H?

The answer is "W–TiC/H will be more useful". Because (1) Hydrogen is easily removed from HIPed compacts than Ar, leading to higher densification. (2) Retained Ar collects and forms bubbles, which reduce the thermal conductivity and enhance surface exfoliation and cracking due to high heat loading by e-beams and due to high energy He ion irradiation. (3) HIPing at an increased pressure of 1 GPa can significantly suppress Ar bubble formation relative to that of 0.2 GPa, but such a HIPing operation should not be considered as the primary processing option for an econom-

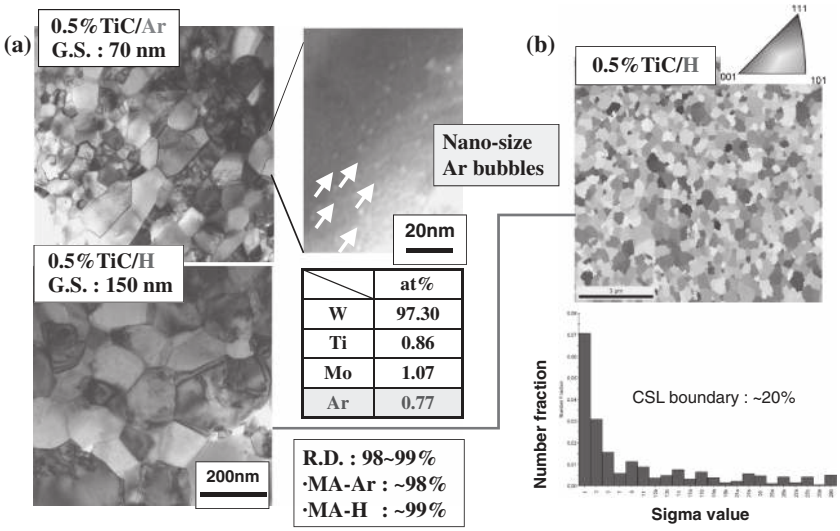

Fig. 1 TEM bright field images depicting the grain structures of UFGR W–0.5TiC/H and W–0.5TiC/Ar together with an enlarged micrograph and EDX results for W–0.5TiC/Ar[23] and EBSP results on grain boundary orientation in W–0.5TiC/H. G.S. and R.D. stand for the average grain size and relative density, respectively.

ical reason. (4) W–TiC/H exhibits better thermo-mechanical properties than W–TiC/Ar mainly due to the existence of Ar bubbles.

3.1 Microstructures

(1) Grains:[23,25,29] TEM (Transmission Electron Microscopy) observations show that the UFGR W–TiC exhibits equiaxed grains in the recrystallized state. TiC addition, even with 0.25 mass%, has a significant effect of grain refinement. The average grain size is in a range of 50 to 200 nm depending on the atmosphere in MA and TiC addition: The grain size in W–TiC/Ar is approximately one half of that in W–TiC/H, probably due to the effect of residual, nano-size Ar bubbles (Fig. 1(a)[23]) which likely give the pinning effect similar to fine dispersoids and inhibit grain growth. The Ar bubbles are formed in W–TiC/Ar and derived from a minute amount of the tightly contained Ar residue left in the MA powder. Such bubbles are, however, invisible in W–TiC/Ar HIPed at an increased pressure of 1 GPa and 1673 K. This observation is consistent with the evidence that the measured density of the W–TiC/Ar HIPed at 1 GPa is approximately equal to the theoretical density. However, it is not clear at present whether or not the content of residual Ar in W–TiC/Ar is affected by HIPing pressure.

(2) Grain boundary orientation: EBSP (Electron Backscatter Diffraction Pattern) shows that the distribution of the grain boundary orientation (misorientation between adjacent grains) obeys the Mackenzie curve based on the random distribution of grain orientation. The fraction of the CSL (coincidence-site lattice) grain boundaries of Σ1 to Σ29b is only 20% in total and most of the grain boundaries are random grain boundaries of high energy (Fig. 1(b)).

(3) Dispersoid: X-ray diffraction (XRD) analyses show that the dispersoids are TiC. However, when the UFGR W–TiC contains a considerable amount of oxygen impurity, e.g., ~800 wtppm, the W_2C phase appears, due to the preferential reaction of titanium with oxygen to forms a titanium oxide and the resultant reaction of the residual carbon atoms with the surrounding W atoms. As a result, the amount of the TiC phase decreases with increasing oxygen content. It should be noted that the enrichment of TiC offers a beneficial effect of strengthening random grain boundaries, whereas the W_2C phase will act as sites susceptible to cracking. Uncombined, free oxygen would segregate at grain boundaries, promoting intergranular brittleness.

TEM observations on the TiC phase showed that the TiC dispersoids are distributed in the grain interior and at the grain boundaries, and the average size of the dispersoids is approximately 15 nm in the grain interior and 30 nm at the grain boundaries. As is typical of precipitates, the dispersoids exhibit a preferable orientation relationship with the matrix phase: The Kurdjumov-Sachs (K-S) orientation relationship at the interface between the TiC phase and W matrix[21] meets

$$(111)\text{fcc} \;//\; (110)\text{bcc},\ [1\bar{1}0]\text{fcc} \;//\; [1\bar{1}1]\text{bcc}.$$

3.2 Mechanical properties[23,29,30]

The yield and fracture strengths and the ductile brittle transition temperature (DBTT) defined as the nil ductility temperature, were measured by three-point bending tests. The fracture strength was estimated to be the maximum fiber stress given by

$$\sigma = 3LS/2WT^2.$$

Here, σ is the stress, L is the applied load, S is the span, W and T are the specimen width and thickness, respectively.

As shown in Fig. 2,[30] the fracture strength at room temperature depends on TiC addition, MA atmosphere and HIP pressure. TiC addition of 0.25% significantly increases the fracture strength to ~1.3 GPa for W–TiC/Ar and ~2 GPa for W–TiC/H. However, further TiC additions to 1.5% do not change the fracture strength. For the W–TiC/Ar, HIPing at the increased pressure of 1 GPa (UH) increases the fracture strength to 2.6 GPa mainly due to the significant suppression of the nano-sized Ar bubbles, while for W–TiC/H no strength increase is recognized. A noted feature for both W–TiC/Ar and W–TiC/H is that no appreciable ductility occurs at room temperature and the DBTT is as high as

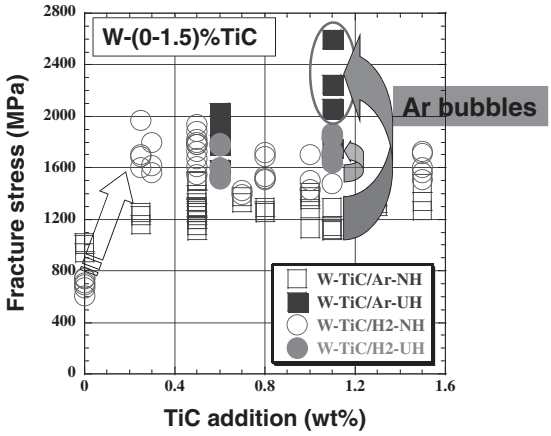

Fig. 2 Effects of TiC addition, MA atmosphere and HIP pressure on three-point bend fracture strength at room temperature and 5×10^{-3} mm/s for UFGR W–(0–1.5)%TiC (/H and /Ar). NH stands for HIP at a normal high pressure of 0.2 GPa and UH HIP at an ultra high pressure of 1 GPa.

$\gtrsim$830 K. This is mainly because the yield strength of the UFGR W–TiC is extremely high owing to the Hall Petch effect and hence the highest fracture strength ($\sim$2.6 GPa) is still much below the yield strength.

3.3 Thermal properties[29)]

The coefficients of thermal expansion (CTEs) and thermal conductivities of UFGR W–TiC/H and stress relieved pure W (W/SR) were measured from 300 to 1800 K. The CTEs of both materials are nearly the same in the measured temperature range and slightly increase with increasing temperature. On the other hand, the thermal conductivities depend on temperature differently each other: For the pure W/SR the thermal conductivity shows the well known temperature dependence, decreasing from 160 W/mK at 300 K to 100 W/mK at 1800 K, while for the W–TiC/H it is almost independent of temperature, staying at approximately 100 W/mK. The values of both materials come closer as the temperature increases. The less temperature dependent thermal conductivity for W–TiC/H is attributable to the high density of grain boundaries and dispersoids.

3.4 Irradiation behavior

(1) Neutron irradiation:[21,25,29)] The UFGR W–TiC (/H and /Ar) and commercially available pure W/SR were irradiated with neutrons at 563 and 873 K up to 2×10^{24} n/m^2 ($E_n > 1$ MeV) in JMTR (Japan Materials Testing Reactor). The irradiation causes microstructural changes and radiation hardening, but the degrees of the microstructural changes and radiation hardening for the UFGR W–TiC (/H and /Ar) are significantly reduced compared with those for the pure W/SR, owing to the beneficial effect of a high density of sinks introduced in UFGR W–TiC (/H and /Ar). Irradiation-induced voids were formed under the 873 K-irradiation and their number density is much lower in UGFR W–TiC (/H and /Ar) than in pure W/SR. No significant difference in radiation resistance between UFGR W–TiC/H and W–TiC/Ar is recognized, indicating that the Ar bubbles do not give a substantial effect on the formation of radiation induced defects.

(2) Helium irradiation:[25,26,29)] Irradiation with 3 MeV $^4He^+$ was conducted at 300, 673 and 823 K up to $\sim 3 \times 10^{23}$ He/m^2 for UFGR W–TiC and commercially available W materials, such as pure W and K-doped W that are in the stress relieved (W/SR) and recrystallized (W/R) states. The UFGR W–TiC/H exhibits no exfoliation and surface cracks at 673 and 773 K, whereas the commercially available W materials exhibit significant exfoliation and surface cracks along grain boundaries even after irradiation of $\sim 2 \times 10^{22}$ He/m^2. Radiation hardening for UFGR W–TiC (/H and /Ar) is much less than that in the commercially available W materials. The superior surface damage resistance for the UFGR W–TiC/H can be attributed to a wide distribution of implanted He by enhanced diffusion along grain boundaries in UFGR W–TiC/H, which suppresses accumulation of He and hence surface exfoliation and hardening. On the other hand, the UFGR W–TiC/Ar exhibits less surface damage resistance. This suggests that the Ar bubbles in W–TiC/Ar act as trapping sites for implanted He.

(3) Low-energy hydrogen irradiation:[22,29)] Irradiation with 1 keV H^{3+} containing $\sim$0.8%C was carried out at 653 K to 10^{25} H/m^2 for UFGR W–TiC/H and commercially available pure W/SR, W/R and La_2O_3 doped W (W–La_2O_3). The UFGR W–TiC/H exhibits a preferable feature from the viewpoint of hydrogen blistering, in comparison with the commercially available W materials: The latter shows blistering and surface exfoliations at 653 K, whereas the UFGR W–TiC/H does not show significant blistering but show many small holes (see Figs. 7(a)–7(d)). The absence of blistering in UFGR W–TiC/H can be attributed to a wide distribution of introduced hydrogen by enhanced diffusion along the grain boundaries in the ultra-fine grains. On the other hand, small holes were not observed in commercially available W materials. The hole formation in the W–TiC/H is most likely a result from ejection of fine grains due to accumulation of hydrogen at grain boundaries very close to the specimen surface and insufficient strengthening of random grain boundaries, or insufficient enrichment of TiC at random grain boundaries.

3.5 Response to thermal shock loading[32)]

Thermal shock tests were conducted by pulsed electron beam heating under the condition of ITER-ELM (Edge-Localized Mode) like loding, where t (pulse length) = 1 ms, P (heat density) = 1.1 GW/m^2 (ΔT (resultant surface temperature increase) $\approx$ 2270 K), T_{base} (base temperature) = 373 K, n (repeated pulse number) = 100, by using JUDITH (JUelicher DIvertor Test facility in Hot cells)-1 operating at FZK in Germany. The irradiated region was the central area of the specimen, approximately 4 mm $\times$ 4 mm. The UFGR W–TiC/H exhibits net-pattern like cracks on the surface and a semi-circle in the interior with a maximum depth of 0.17 mm (see Fig. 8) which were caused by thermal internal stresses generated by a temperature gradient in the specimen.

3.6 A new method (GSMM) to solve the problems in UFGR W–TiC

The above features in UFGR W–TiC contain the following problems:

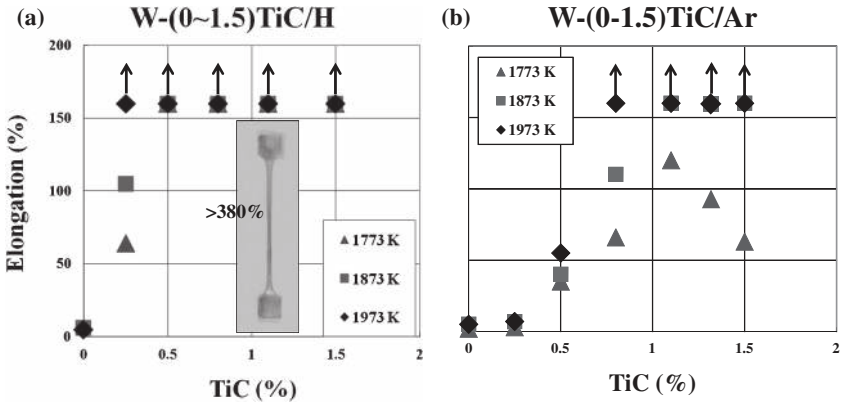

Fig. 3 Tensile elongation at 1773, 1873 and 1973 K at an initial strain rate of $5 \times 10^{-4}\,s^{-1}$ as a function of TiC content: (a) W–(0–1.5)TiC/H and (b) W–(0–1.5)TiC/Ar. The arrows indicate the elongation exceeding 160%.

(1) High DBTT and not very high fracture strength.
(2) Less thermal conductivity at RT-1600 K than ITER grade W/SR.
(3) Many small surface holes caused by low-energy hydrogen irradiation.
(4) Thermal shock cracking under ITER/ELM like loading with JUDITH-1.

It should be noted that most of the above problems (items (1), (3) and (4)) are ascribed mainly to insufficient strengthening of the high-energy random grain boundaries in UFGR W–TiC (/H and /Ar). The insufficient strengthening stems from insufficient precipitation of TiC and segregation of the TiC constituents at the random grain boundaries. In addition to the insufficient grain boundary strengthening, the high DBTT of UFGR W–TiC (/H and /Ar) is also attributed to extremely high yield strength due to grain size strengthening, and the existence of residual pores of 1–2% (residual pores are defined as the pores of residual gases). It is thus required to enhance the precipitation of TiC and segregation of the TiC constituents at the random grain boundaries, grow the grains to appropriate sizes to reduce the extremely high yield strength to the required level and thoroughly remove the residual pores. For this purpose, a microstructural modification method has been newly developed.

This method is based on activation of grain boundary sliding by superplastic deformation, where the recrysallized state and equiaxed grain geometry are maintained and the deformation is driven by active grain rotation and extensive relative displacement of the adjacent grains accompanied with moderate grain growth.[33] These grain boundary activities would lead to the optimization of precipitation of TiC and segregation of the TiC constituents at the random grain boundaries (see Fig. 7), thereby strengthening the grain boundaries with holding the recrystallized state. The method may also have the effects of removing Ar in the residual pores through grain boundary diffusion during the deformation driven by active grain rotation and extensive relative displacement of the adjacent grains and decreasing the yield strength to appropriate values. This new method is designated as GSMM (Grain boundary Sliding-based Microstructural Modification).

3.7 Superplastic behavior of UFGR W–TiC[20,23,24,27,29]

The benefit of GSMM can be fully utilized when the UFGR W–TiC exhibits superplastic deformation with sufficiently large elongation and relatively low flow resistance without crack formation and its linkage. In order to find the optimum deformation condition for GSMM, the superplastic behavior of UFGR W–TiC has been extensively studied as a function of TiC content, MA atmosphere, temperature and strain rate. The main results are as follows:

(1) The superplastic behavior of UFGR W–TiC depends significantly on TiC content, MA atmosphere, temperature and strain rate.

(2) The elongation to fracture for MA-HIPed W compacts without TiC addition is very small even at 1973 K, but it significantly increases with increasing TiC addition and takes a maximum at the TiC addition of ~1.1% (Fig. 3).

(3) The flow stress depends strongly on temperature and strain rate and decreases to relatively low values at and above 1873 K and below $\sim 1 \times 10^{-3}\,s^{-1}$, but is less dependent on TiC addition and MA atmosphere.

(4) Residual Ar results in decrease of the elongation, flow stress and the strain rate sensitivity of flow stress (*m*-value). TiC addition offsets the ductility reduction caused by the Ar bubbles.

(5) The elongation, flow stress and *m*-value can be optimized by TiC addition and MA atmosphere.

(6) The major contribution of TiC is to suppress crack formation and its linkage at weak grain boundaries due to grain boundary sliding.

(7) The activation energy for deformation determined is close to that for grain boundary diffusion in UFGR W–TiC.

4. Toughened, Fine-Grained, Recrystallized (TFGR) W–1.1%TiC

Since the TiC addition of ~1.1% was found to provide the highest elongation and relatively low flow resistance above 1873 K,[27] GSMM treatments by compression were applied to UFGR W–1.1TiC (/H and /Ar) as a function of GSMM temperature and reduction ratio. It is found that GSMM treatments for UFGR W–1.1TiC (/H and /Ar) lead to significant strengthening of the grain boundaries and hence decrease in the DBTT down to room temperature or less.

The GSMM treated W–1.1TiC is designated as toughened, fine-grained, recrystallized W–1.1%TiC (TFGR W–1.1TiC). The TFGR W–1.1TiC compacts were subjected to micorstructural examinations, mechanical and thermal property evaluations, thermal shock and thermal fatigue loadings and low-energy plasma exposure. The followings are the main results obtained through domestic and international research collaborations on TFGR W–1.1TiC.

4.1 Mechanical properties

4.1.1 Behavior at room temperature[30,34–36)]

Three-point bending tests were conducted at room temperature on W–1.1TiC (/H and /Ar) before and after GSMM, and the results of fracture strength for W.1.1TiC/Ar are shown in Fig. 4. It should be noted that GSMM treatments for the as-HIPed specimens significantly increase the fracture strength: In particular, for the specimens HIPed at 1 GPa (W–1.1TiC/Ar-UH) and GSMM treated at 1923 K to ~80% in reduction ratio, the fracture strength increases from 2.4 to 4.4 GPa. To the best of the authors' knowledge, this RT fracture strength is the highest among the W materials reported so far.

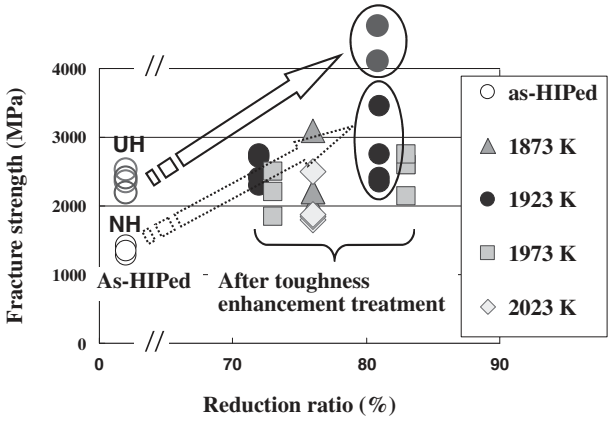

Fig. 4 Effects of GSMM temperature and reduction ratio in compression on three-point bend fracture strength at room temperature and 5.0×10^{-3} mm/s for W–1.1TiC/Ar-NH and W–1.1TiC/Ar-UH. NH and UH stand for HIP at 0.2 and 1.0 GPa, respectively.

The significantly increased strength up to this level is accompanied by an appreciable plastic strain prior to fracture. Figure 5 shows three-point bending stress–strain curves for W–1.1TiC/Ar-UH and W–1.1TiC/H–NH (HIP pressure: 0.2 GPa) before and after GSMM treated at 1923 K and ~80% in reduction ratio. The arrows indicate the proportional limit. W–1.1TiC/H–NH exhibits appreciably larger plastic strain and lower yield and fracture strengths than W–1.1TiC/Ar-UH. This is due to strengthening of random grain boundaries concomitant with reduction in the yield strength followed by a lower work hardening rate, which reflects a larger grain size in W–1.1TiC/H (~1.5 μm) than W–1.1TiC/Ar (~0.5 μm) as shown in Fig. 6.

SEM micrographs of fracture surfaces are included in Fig. 5. It appears that both specimens fracture not only intergranularly, but also transgranularly. According to the low magnification micrograph in W–1.1TiC/Ar-UH where the fracture initiation site (river pattern) is encircled, fracture appears to originate at a stress concentrator like an inclusion. This implies that the intrinsic fracture strength of W–1.1TiC/Ar-UH without such stress concentrators should exceed the measured value of 4.4 GPa, providing evidence of the significant strengthening of the random grain boundaries by GSMM.

4.1.2 DBTT

In order to measure the DBTT as a function of impurity contents of oxygen and nitrogen, UFGR W–1.1TiC/H with different contents of oxygen and nitrogen were subjected to GSMM at 1923 K to ~80% and then three-point bending tests. The values of plastic strain up to fracture were plotted against temperature and extrapolated to zero to determine the temperature where plastic strain begins to appear, i.e., the DBTT. The DBTT of GSMM treated W–1.1TiC/H is strongly dependent on the contents of oxygen and nitrogen, especially on oxygen content. The DBTT decreases with decreasing oxygen content and is between 240 and 420 K for oxygen contents of 160–870 wppm. Since the DBTT of UFGR W–1.1TiC/H is ~830 K, it should be noted that GSMM leads to significant decrease in DBTT, an approximate reduction by 590 K for the specimen with 160 wppm oxygen.

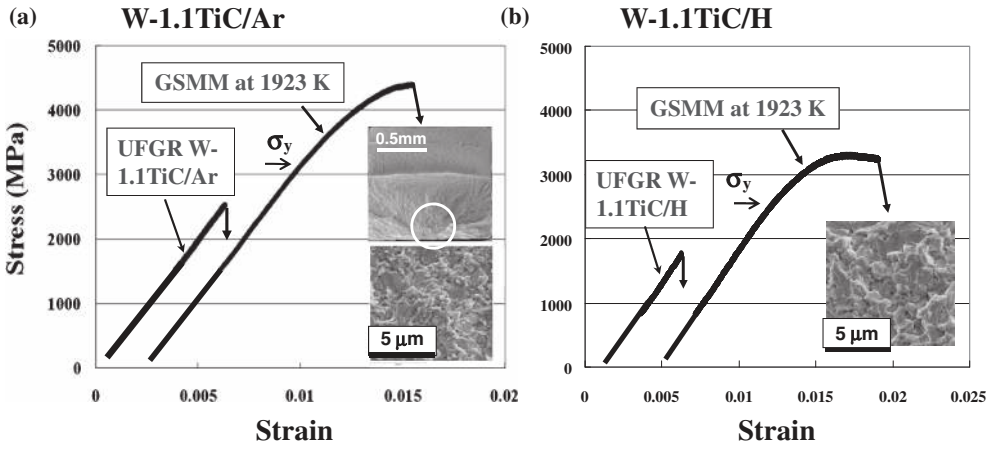

Fig. 5 Three-point bend stress strain curves at room temperature and 5×10^{-3} mm/s for (a) W–1.1TiC/Ar-UH and (b) W–1.1TiC/H–NH before and after GSMM at 1923 K to approximately 80% in reduction ratio. σy indicates the proportional limit (yield stress). UH and NU stand for HIP at 1 and 0.2 GPa, respectively. SEM micrographs of fracture surface are also shown.

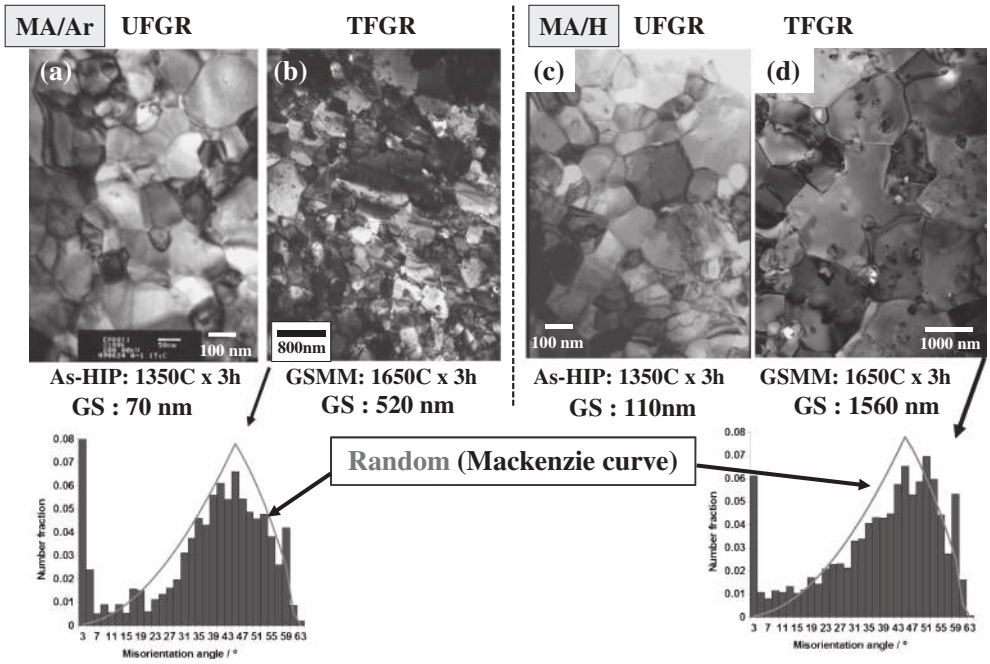

Fig. 6 TEM bright field images depicting the grain structures in UFGR and TFGR W–1.1TiC/Ar-UH and W–1.1TiC/H–NH together with EBSP results on grain boundary orientation of TFGR W–1.1TiC/Ar-UH and W–1.1TiC/H–NH. G.S. stands for the average grain size.

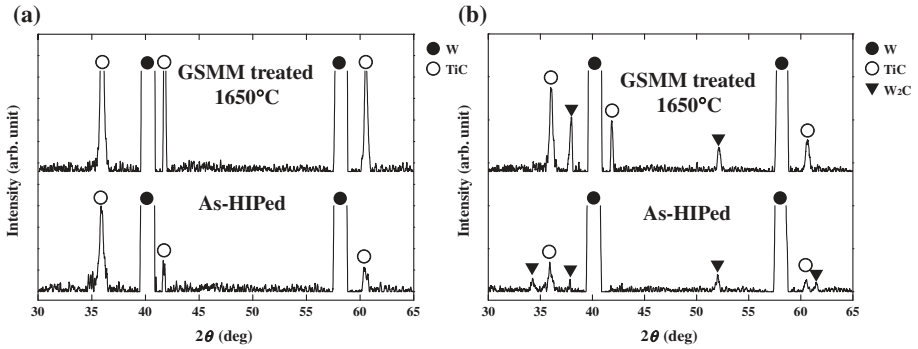

Fig. 7 Comparison of XRD patterns between TFGR and UFGR W–1.1TiC/H with (a) low (160 mass ppm) and (b) high oxygen (850 mass ppm) contents.

As mentioned in section 3.1, increase in oxygen content leads to the formation of the W_2C phase. XRD analyses showed that GSMM treated W–1.1TiC/H contains an increased amount of W_2C and decreased amount TiC for the specimen with high oxygen contents (Fig. 7). W_2C is known to be a brittle phase and may act as initiation sites of cracking. It is likely that an excessive amount of oxygen disturbs the recombination of decomposed TiC through the formation of a Ti oxide and the W_2C phase.

4.2 Microstructures

Figure 6 shows TEM microstructures and grain boundary orientations analyzed by EBSP for UFGR and TFGR W–1.1TiC (/H and /Ar) shown in Fig. 5. Leaving the grain shape equiaxed, GSMM treatments increase the grain size almost by one order; the grain size is 0.5 μm for W–1.1TiC/Ar and 1.5 μm for W–1.1TiC/H.[30,35,37] The distribution of grain boundary orientation obeys the Mackenzie curve based on the random distribution of grain orientation in both TFGR (/H and /Ar), indicating that most of the grain boundaries are random grain boundaries of high energy. No visible nano-sized bubbles are observed in TFGR W–1.1TiC/Ar-UH as well as in TFGR W–1.1TiC/H–NH. This is because the TFGR W–1.1TiC/Ar-UH was subjected to HIP at 1 GPa (UH) and exhibits an increased relative density.

Promoting segregation and precipitation of TiC, GSMM treatments significantly increased the amount of dispersoids (see Fig. 7). The average size of the dispersoids for TFGR W–1.1TiC/H reaches 90 nm in the grain interior and 160 nm at the grain boundaries.[32,35] This indicates that the effect of GSMM is significant for TiC precipitation and its segregation at the random grain boundaries. As the GSMM temperature increases, the average size increases: The average size for W–1.1TiC/H–NH with GSMM at 2270 K increases to 160 nm in the grain interior and 390 nm at the grain boundaries.[32] In those GSMM treated specimens, the Kurdjumov-Sachs (K-S) orientation relationship is recognized at the interface between the TiC phase and W matrix.

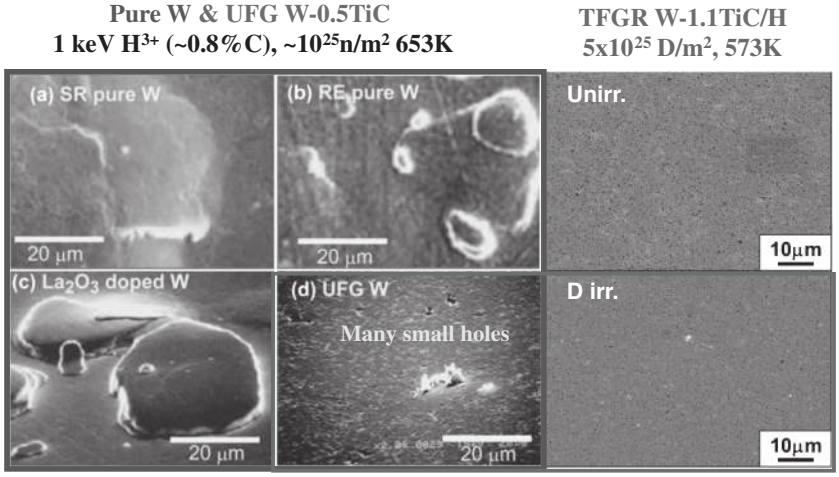

Fig. 8 SEM micrographs of surfaces of (a) pure W/SR, (b) pure W/R, (c) La_2O_3 doped W and (d) UFGR W–0.5TiC after irradiation with 1 keV H^{3+} (~0.8%C) to $\sim 10^{25}$ n/m^2 at 653 K and of TFGR W–1.1TiC/H before and after irradiation of ~55 eV D plasma to 5×10^{25}/m^2 at 573 K.

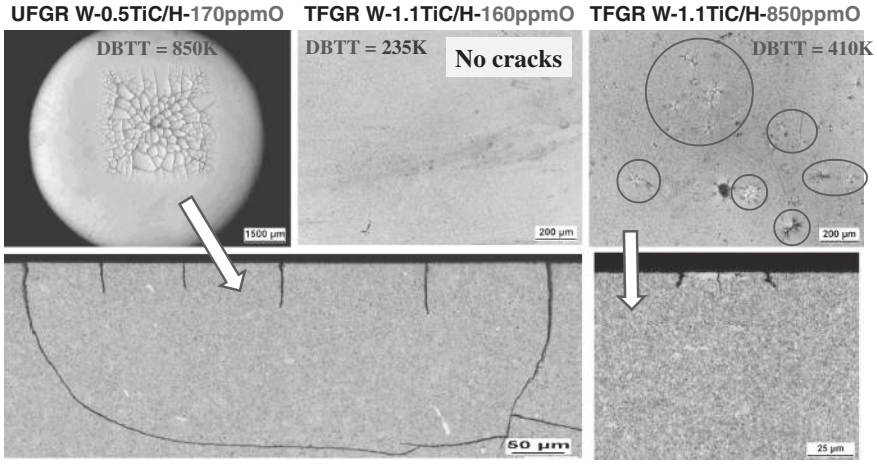

Fig. 9 Optical micrographs of UFGR W–0.5TiC/H and TFGR W–1.1TiC/H with 160 and 850 mass ppm in oxygen contents after thermal shock loading; top surface view (top) and representative cross sectional view (bottom). The DBTT is included in the figure.

4.3 Low-energy D plasma exposure[38)]

Pure W/SR, W/R and TFGR W–1.1TiC (/H and /Ar) were exposed to pure D and mixed species D + 20%He plasmas with low energy ($\sim 55 \pm 15$ eV), high flux ($\sim 10^{22}$ m^{-2} s^{-1}), high fluence (4.5×10^{26} m^{-2}) at ~573 K in the linear divertor plasma simulator PISCES-A at the University of California, San Diego. The results show that W–1.1TiC/Ar-UH and W–1.1TiC/H-UH exhibit superior performance to W/SR and W/R; no holes and no blisters are formed (Fig. 8), and D retention is much less than those in W/SR and W/R of $\sim 10^{21}$ m^{-2} by around two orders of magnitude. The observed superior properties of TFGR W–1.1TiC (/H and /Ar) can be attributed not only to their much finer grain size than that of W/SR and W/R, but also to the modified microstructure where the random grain boundaries in the recrystallized state are significantly strengthened.

4.4 Thermal shock loading[32)]

TFGR W–1.1TiC/H with two different oxygen contents of 160 and 850 wppm were subjected to thermal shock tests with JUDITH-1 under the condition of ITER-ELM same as for UFGR W–TiC/H (oxygen content: 170 wppm). The result is shown in Fig. 9 together with that for UFGR W–0.5TiC/H. It should be noted that no cracks are observed on the surface of TFGR W–1.1TiC/H with 160 ppm oxygen, although very shallow cracks are observed on the surface of TFGR W–1.1TiC/H with 850 ppm oxygen. TFGR W–1.1TiC/H with 160 ppm oxygen, even when the base temperature was decreased from 373 K to room temperature, did not exhibit any cracks on the surface.

4.5 Thermal fatigue loading[39)]

TFGR W–1.1TiC/H and commercially available pure W/SR were subjected to thermal fatigue tests by electron beam irradiation with the following two heating patterns imposed consecutively; (1) surface temperature of around 1973 K, duration of 180 s and (2) repeated irradiations of 2 s-irradiation and 8 s-rest in one cycle of 10 s for totally 1 h resulted in temperature variation between 1523 and 723 K with 380 cycles. For W/SR, the irradiation around 1973 K causes recrystallization and grain growth that decrease the

yield stress and promote cracking at grain boundaries (recrystallization embrittlement), resulting in significant surface roughening (plastic deformation), localized small cracking at grain boundaries and surface exfoliation. The subsequent repeated irradiation aggravates surface roughening and cracking. On the other hand, TFGR W–1.1TiC/H does not exhibit any surface roughening and cracking. The observed noticeable difference in the thermo-mechanical properties between W/SR and TFGR W–1.1TiC/H can be attributed to the difference in dynamic yield strength and grain boundary strength: TFGR W–1.1TiC/H exhibits much higher dynamic yield strength due to fine grains (Hall Petch effect) and much higher grain boundary strength due to enrichment with TiC and its constituents.

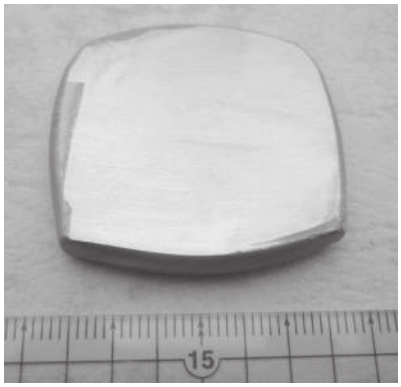

Fig. 10 Optical micrograph of TFGR W–1.1TiC/H with the dimensions equivalent to a piece of divertor tile in ITER.

4.6 Thermal property[32)]

The thermal conductivity of TFGR W–1.1TiC/H was measured up to 1500 K and compared with that of UFGR W–TiC/H. No difference in thermal conductivity between the two is recognized, indicating that GSMM does not change the thermal conductivity of UFGR W–TiC/H.

5. Application of TFGR W–1.1TiC to Divertor in ITER

5.1 Fabrication of divertor tile in ITER with TFGR W–1.1TiC/H

The required dimensions of the divertor tiles in ITER are approximately 30 mm × 30 mm × 12 mm. The present fabrication method, i.e., the MA-HIP-GSMM route is applicable to the fabrication of a plate of TFGR W–1.1TiC/H with such dimensions. Figure 10 shows an example of a TFGR W–1.1TiC/H compact having dimensions satisfactory as a divertor tile. The TFGR W–1.1TiC/H compact will behave as described in sections 4.1–4.5 since the oxygen and nitrogen contents are maintained to be sufficiently low.

5.2 Remaining issues in TFGR W–1.1TiC

From engineering viewpoints including ITER applications as well as scientific viewpoints, it is important to fully recognize the issues remained in TFGR W–1.1TiC.

One is to elucidate the cause of lower thermal conductivity in TFGR W–1.1TiC to increase the thermal conductivity, as mentioned in section 4.6. Enhancement of thermal conductivity will further improve the surface damage resistance to thermal shock and thermal fatigue loading.

Another issue is the retention of hydrogen isotopes which is important for safety assessment of fusion reactors since radioactive tritium is a hydrogen isotope. Two conflicting results have been reported concerning the retention of the isotopes in TFGR W–1.1TiC relative to those in commercially available W (W/SR and W/R). One result[38)] confirms lower retention in TFGR W–1.1TiC but the other indicates higher retention.[40)] There are two possible explanations for this. One is the effect of a difference in microstructure between the TFGR W–1.1TiC specimens used in each experiment; the lower retention in TFGR W–1.1TiC is observed for a precursory compact HIPed at 1.0 GPa and 1673 K (W–1.1TiC/Ar-UH, W–1.1TiC/H-UH) and then GSMM treated, while the higher retention is for that HIPed at 0.2 GPa and 1623 K (W–1.1TiC/H–NH) and then GSMM treated. HIPing at the higher pressure and higher temperature is effective in significantly suppressing the residual pores. The other explanation is due to different irradiation conditions; the lower retention is observed for high flux ($\sim 10^{22}\,m^{-2}s^{-1}$) and high fluence ($4.5 \times 10^{26}\,m^{-2}$) in PISCES-A, while the higher retention for low or mediate flux and low or mediate fluence. Further studies should be needed to fully explain the two conflicting results on the retention of hydrogen isotopes.

5.3 TFGR W based materials with addition of another TMC

The microstructures and the observed superior properties of TFGR W–1.1TiC owe to the beneficial effects of TiC additions via TiC precipitation and its segregation at the random grain boundaries in the recrystallized state. Under the fusion reactor environment of the steady-state and pulsed fluxes of heat and particles, however, once the surface temperature of TFGR W–1.1TiC is increased to the temperatures where TiC forms a eutectic with W or begins to melt, the benefit of TiC addition will be lost. It is hence required to explore additions of other TMCs that are more thermally stable than TiCx with higher eutectic temperatures and higher melting points. Among the TMCs, TaCx was selected and TFGR W–3.3%TaC compacts were fabricated by the MA-HIP-GSMM method. TaCx has a much higher melting point (~4200 K) than TiCx (~3500 K) or W (~3700 K) and 3.3%TaC provides the same molar fraction as 1.1%TiC. Promising results with TaC addition, or reduction of DBTT, has been also reported for Mo belonging to the same VIA group as W.[16)] Studies on TFGR W–3.3%TaC/H are now in progress, focusing on its response to thermal shock loading and hydrogen isotope retention under an ITER-like environment.

6. Summary

This paper has made an extensive review of our nanostructured tungsten (W) based materials development performed so far to significantly mitigate recrystallization- and radiation-induced embrittlement, including new original results. The basic approach to the mitigation is to seek the most preferable microstructure that is composed of a high density of both the dispersoids of transition metal carbides

(TMCs) such as TiCx and random grain boundaries (GBs) in the recrystallized state. The GBs are significantly strengthened by precipitation of TMCs and segregation of the TMC constituents at the boundaries. We fabricated ultra-fine grained (UFGR), recrystallized W–(0.25–1.5)%TiC compacts by powder metallurgical methods utilizing MA and HIP. The UFGR W–(0.25–1.5)%TiC exhibits favorable as well as unfavorable features of the microstructures, mechanical and thermal properties and responses to neutron and ion irradiation, plasma exposure and high heat loading.

Most of the unfavorable features stem from insufficient strength of random GBs in the recrystallized state. In order to substantially strengthen the random GBs in UFGR W–TiC, a new microstructural modification method has been developed. The method is based on activation of GB sliding which leads to significant strengthening of random GBs by enhancing the precipitation of TiCx and segregation of the TiCx constituents at the GBs, and is designated as GSMM (Grain boundary Sliding-based Microstructural Modification).

The optimal application of GSMM under superplastic deformation enables the conversion of the UFGR W–1.1%TiC to toughened, fine-grained, recrystalliged W–1.1%TiC (TFGR W–1.1TiC). TFGR W–1.1TiC exhibits much improved thermo-mechanical performances to thermal shock and thermal fatigue loading, irradiation, etc.

TFGR W–1.1TiC is available as a tile in the ITER divertor by the present MA-HIP-GSMM route. In order to solve the several remaining problems of TFGR W–1.1TiC R & D on TFGR W with additions of TaC that is more thermally stable than TiCx is in progress.

Acknowledgements

The present work was supported by Grant-in-Aid for Scientific Research (B) (#19360412, #22360388), Japan Society for the Promotion of Science (JSPS), which is greatly appreciated.

REFERENCES

1) M. Rieth *et al.*: J. Nucl. Mater. **432** (2013) 482–500.
2) M. Kawai, H. Kurishita, H. Kokawa, S. Watanabe, N. Sakaguchi, K. Kikuchi, S. Saito, T. Yoshiie, H. Iwase, T. Ito, S. Hashimoto, Y. Kaneko, M. Futakawa and S. Ishino: J. Nucl. Mater. **431** (2012) 16–25.
3) S. Suzuki, K. Ezato, Y. Seki, K. Mohri, K. Yokohama and M. Enoeda: Fusion Eng. Design **87** (2012) 845–852.
4) Y. Ueda, H. T. Lee, N. Ohno, S. Kajita, A. Kimura, R. Kasada, T. Nagasaka, Y. Hatano, A. Hasegawa, H. Kurishita and Y. Oya: Phys. Scr. **T145** (2011) 014029.
5) G. S. Bauer: J. Nucl. Mater. **398** (2010) 19–27.
6) T. McManamy, M. Rnnich, F. Gallmeier, P. Furguson and J. Janney: J. Nucl. Mater. **398** (2010) 35–42.
7) For instance, H. Ullmaier and F. Carsughi: Nucl. Instrum. Meth. Phys. Res. B **101** (1995) 406–421.
8) ITER Material Assessment Report 2004 G 74 MA 10 W 0.3.
9) Y. Kitsunai, H. Kurishita, T. Shibayama, M. Narui, H. Kayano and Y. Hiraoka: J. Nucl. Mater. **239** (1996) 253–260.
10) H. Kurishita, Y. Kitsunai, T. Kuwabara, M. Hasegawa, Y. Hiraoka, T. Takida and T. Igarashi: J. Plasma Fusion Res. **75** (1999) 594–603.
11) H. Kurishita: *Basic Studies in the Field of High-Temperature Engineering*, (OECD, 2002) pp. 103–112.
12) Y. Kitsunai, H. Kurishita, T. Kuwabara, M. Narui, M. Hasegawa, T. Takida and K. Takebe: J. Nucl. Mater. **346** (2005) 233–243.
13) H. Kurishita and H. Yoshinaga: Mater. Forum **13** (1989) 161–173.
14) H. Kurishita, Y. Kitsunai, Y. Hiraoka, T. Shibayama and H. Kayano: Mater. Trans. JIM **37** (1996) 89–97.
15) H. Kurishita, Y. Kitsunai, T. Shibayama, H. Kayano and Y. Hiraoka: J. Nucl. Mater. **233–237** (1996) 557–564.
16) T. Takida, H. Kurishita, M. Mabuchi, T. Igarashi, Y. Doi and T. Nagae: Mater. Trans. **45** (2004) 143–148.
17) Y. Kitsunai, H. Kurishita, H. Kayano, Y. Hiraoka, T. Igarashi and T. Takida: J. Nucl. Mater. **271–272** (1999) 423–428.
18) J. S. Benjamin: Met. Trans. **5** (1970) 2943.
19) Y. Ishijima, H. Kurishita, H. Arakawa, M. Hasegawa, Y. Hiraoka, T. Takida and K. Takebe: Mater. Trans. **46** (2005) 568–574.
20) H. Kurishita, S. Kobayashi, K. Nakai, H. Arakawa, S. Matuso, T. Takida, K. Takebe and M. Kawai: Phys. Scr. **T128** (2007) 76–80.
21) H. Kurishita, Y. Amano, S. Kobayashi, K. Nakai, H. Arakawa, Y. Hiraoka, T. Takida, K. Takebe and H. Matsui: J. Nucl. Mater. **367–370** (2007) 1453–1457.
22) Y. Ueda, N. Ohno, S. Kajita, H. Kurishita, H. Iwakiri, K. Tokunaga and N. Yoshida: Fusion Sci. Technol. **52** (2007) 513–520.
23) H. Kurishita, S. Matsuo, H. Arakawa, S. Kobayashi, K. Nakai, T. Takida, K. Takebe and M. Kawai: Mater. Sci. Eng. A **477** (2008) 162–167.
24) S. Matsuo, H. Kurishita, H. Arakawa, T. Takida, M. Kato, Y. Yamamoto, K. Takebe, M. Kawai and N. Yoshida: Mater. Sci. Eng. A **492** (2008) 475–480.
25) H. Kurishita, S. Kobayashi, K. Nakai, T. Ogawa, A. Hasegawa, K. Abe, H. Arakawa, S. Matsuo, T. Takida, K. Takebe, M. Kawai and N. Yoshida: J. Nucl. Mater. **377** (2008) 34–40.
26) T. Ogawa, A. Hasegawa, H. Kurishita and S. Nogami: J. Nucl. Sci. Tech. **46** (2009) 717–723.
27) H. Kurishita, S. Matsuo, H. Arakawa, M. Narui, M. Yamazaki, T. Sakamoto, S. Kobayashi, K. Nakai, T. Takida, K. Takebe, M. Kawai and N. Yoshida: J. Nucl. Mater. **386–388** (2009) 579–582.
28) K. Tokunaga, T. Fujiwara, K. Ezato, S. Suzuki, M. Akiba, H. Kurishita, S. Nagata, B. Tsuchiya, A. Tonegawa and N. Yoshida: J. Nucl. Mater. **390–391** (2009) 916–920.
29) H. Kurishita, S. Matuso, H. Arakawa, H. Hirai, J. Linke, M. Kawai and N. Yoshida: Adv. Mater. Res. **59** (2009) 18–30.
30) H. Kurishita, S. Matsuo, H. Arakawa, T. Sakamoto, S. Kobayashi, K. Nakai, T. Takida, M. Katoh, M. Kawai and N. Yoshida: J. Nucl. Mater. **398** (2010) 87–92.
31) K. Tokunaga, M. J. Baldwin, R. P. Doerner, D. Nishijima, H. Kurishita, T. Fujiwara, K. Araki, Y. Miyamoto, N. Ohno and Y. Ueda: J. Nucl. Mater. **417** (2011) 528–532.
32) G. Pintsuk, H. Kurishita, J. Linke, H. Arakawa, S. Matsuo, T. Sakamoto, S. Kobayashi and K. Nakai: Phys. Scr. **T145** (2011) 014060.
33) For instance, N. Wakai: J. Japan Inst. **45** (2006) 644–647.
34) Y. Ueda, H. T. Lee, N. Ohno, S. Kajita, A. Kimura, R. Kasada, T. Nagasaka, Y. Hatano, A. Hasegawa, H. Kurishita and Y. Oya: Phys. Scr. **T145** (2011) 014029.
35) L. El-Guebaly, R. Kurtz, M. Rieth, H. Kurishita and A. Robinson: Fusion Sci. Tech. **60** (2011) 185–190.
36) M. Kawai, H. Kurishita, H. Kokawa, S. Watanabe, N. Sakaguchi, K. Kikuchi, S. Saito, T. Yoshiie, H. Iwase, T. Ito, S. Hashimoto, Y. Kaneko, M. Futakawa and S. Ishino: J. Nucl. Mater. **431** (2012) 16–25.
37) M. Kajioka, T. Sakamoto, S. Kobayashi, K. Nakai, H. Kurishita, S. Matsuo and H. Arakawa: J. Nucl. Mater. **417** (2011) 512–515.
38) M. Miyamoto, D. Nishijima, Y. Ueda, R. P. Doerner, H. Kurishita, M. J. Baldwin, S. Morito, K. Ono and J. Hanna: Nucl. Fusion **49** (2009) 065035.
39) K. Tokunaga, H. Kurishita, H. Arakawa, S. Matsuo, T. Hotta, K. Araki, Y. Miyamoto, T. Fujiwara, K. Nakamura, T. Takida, M. Kato and A. Ikegaya: Proceedings of ICFRM-15, (October 16–21. 2011 Charleston, CA, USA), submitted to J. Nucl. Mater.
40) M. Oya, K. Uekita, H. T. Lee, Y. Ohtsuka, Y. Ueda, H. Kurishita, A. Kreter, J. W. Coenen, V. Philipps, S. Brezinsek, A. Litnovsky, K. Sugiyama and Y. Torikai: J. Nucl. Mater. (2013), in press.